Angular Variability of the Liquid Water Cloud Optical Thickness Retrieved from ADEOS–POLDER

JEAN-CLAUDE BURIEZ, MARIE DOUTRIAUX-BOUCHER, AND FRÉDÉRIC PAROL

Laboratoire d'Optique Atmosphérique UMR CNRS, Université des Sciences et Technologies de Lille, Villeneuve d'Ascq, France

NORMAN G. LOEB

Center for Atmospheric Sciences, Hampton University, Hampton, Virginia

(Manuscript received 5 July 2000, in final form 17 February 2001)

ABSTRACT

The usual procedure for retrieving the optical thickness of liquid water clouds from satellite-measured radiances is based on the assumption of plane-parallel layers composed of liquid water droplets. This study investigates the validity of this assumption from Advanced Earth Orbiting Satellite–Polarization and Directionality of the Earth's Reflectances (ADEOS–POLDER) observations. To do that, the authors take advantage of the multidirectional viewing capability of the POLDER instrument, which functioned nominally aboard ADEOS from November 1996 to June 1997.

The usual plane-parallel cloud model composed of water droplets with an effective radius of 10 μm provides a reasonable approximation of the angular dependence in scattering at visible wavelengths from overcast liquid water clouds for moderate solar zenith angles. However, significant differences between model and observations appear in the rainbow direction and for the smallest observable values of scattering angle ($\Theta < 90°$). A better overall agreement would be obtained for droplets with an effective radius of about 7–8 μm for continental liquid water clouds. On the other hand, changing the water droplet size distribution would not lead to a significant improvement for maritime situations. When horizontal variations in cloud optical thickness are considered by using the independent pixel approximation (IPA), a small improvement is obtained over the whole range of scattering angles but significant discrepancies remain for $\Theta < 80°$, that is for large solar zenith angles in the forward-scattering direction. The remaining differences between various models based on the plane-parallel radiative transfer and POLDER observations are thought to be due to variations in cloud shape.

1. Introduction

Clouds, which are the main modulator of the radiation field, may have an important influence on the climate and its variations. Their radiative properties have to be properly modeled in general circulation models as well as for deriving cloud parameters from satellite radiances. Nevertheless, clouds are usually treated as homogeneous plane-parallel layers and are often assumed to be composed of spherical particles with a fixed size distribution, although these assumptions are known to be incorrect.

Cloud optical thickness, which is directly related to the condensed water content, is a key parameter in cloud modeling. It is routinely inferred from radiance measurements, in particular in the context of the International Satellite Cloud Climatology Project (ISCCP) (Rossow and Schiffer 1991). Many theoretical studies have outlined the importance of the hypotheses on cloud microphysics and on the three-dimensional distribution of the water content in the optical thickness retrieval. For liquid water clouds, an error of factor 2 in the droplet radius induces an error in cloud optical thickness of about 10% (Han et al. 1994.) In the case of cirrus clouds, the use of a wrong particle shape model (sphere instead of crystal) can result in an overestimation of the optical thickness by a factor that can exceed 3 (Mishchenko et al. 1996). With regard to the horizontal distribution of the cloud water content, neglecting the heterogeneities can lead to an underestimation of the mean optical thickness by 30% even for flat overcast cloud layers (Cahalan 1994). This departure from the homogeneous plane-parallel model can be highly enhanced because of cloud-top height variations (Loeb et al. 1998).

Unlike the usual scanner radiometers, Polarization and Directionality of the Earth's Reflectances (POLDER; Deschamps et al. 1994) provides up to 14 quasi-simultaneous reflectance measurements of a geographical target. While it is always possible to adjust a cloud model to match one single bidirectional observation of

Corresponding author address: Prof. J.-C. Buriez, Batiment P5, Université des Sciences et Technologies de Lille, 59655 Villeneuve d'Ascq Cedex, France.
E-mail: buriez@univ-lille1.fr

a given target, constraining such a model to adequately match a set of bidirectional observations is much more demanding. Consequently, POLDER not only allows retrieval of cloud optical thickness for some assumed model (e.g., plane-parallel assumption with an assumed droplet size distribution), but it also provides a means of examining the self-consistency in the retrieved optical thicknesses, and thus the validity of the assumed model.

This ability to test cloud models was first demonstrated from measurements acquired by the POLDER airborne simulator during the Atlantic Stratocumulus Transition Experiment (Descloitres et al. 1995) and the European Cloud and Radiation Experiment (Descloitres et al. 1998). The validity of the plane-parallel cloud model was investigated. The standard water droplet cloud model (with an effective radius of 10 μm) used in the ISCCP analysis was found to be suitable for stratocumulus clouds. For cirrus clouds, the ice polycrystal model chosen for the reanalysis of ISCCP (Rossow et al. 1996) appeared highly preferable.

The standard cloud water droplet model is also used in the operational algorithm of the POLDER ''Earth Radiation Budget (ERB) and clouds'' line that derives cloud optical thickness from Advanced Earth Orbiting Satellite (ADEOS)–POLDER data. As expected, first results based on the 10 November 1996 observations over ocean have confirmed that the water droplet model is suitable for liquid water clouds and inadequate for ice clouds (Parol et al. 1999). Since then, several ice cloud particle models were investigated (Doutriaux-Boucher et al. 2000).

This paper focuses on liquid water clouds. Despite a general agreement observed for such clouds from a limited dataset, Parol et al. (1999) outlined a possible weakness of the 10-μm plane-parallel cloud model for values of scattering angle around 80°. That corresponds to large solar zenith angles in the forward direction, which may induce a serious weakness of the plane-parallel approximation as already noted from Advanced Very High Resolution Radiometer (AVHRR) observations (Loeb and Coakley 1998). The aim of this paper is to investigate further the validity of this model for liquid water clouds. Observations sampled throughout the eight months of available ADEOS–POLDER are examined.

Section 2 presents the criteria of selection and the corresponding selected POLDER data. The departure of the observations from the standard plane-parallel model used in the ERB and clouds line is analyzed with respect to different geophysical parameters. The results are reported in section 3. The influence of cloud droplet size and of cloud heterogeneity is considered in sections 4 and 5, respectively. Some conclusions about the plane-parallel approximation are drawn in section 6.

2. Selected POLDER ERB and clouds data

The POLDER instrument functioned nominally aboard ADEOS during 8 months (between November 1996 and June 1997). POLDER is a camera composed of a wide field-of-view (~2200 km) telecentric optics, a rotating wheel carrying spectral filters and polarizers, and a charged coupled device (CCD) array of 242 × 274 detectors that induces a moderate spatial resolution of 6.2 km. POLDER was in a sun-synchronous orbit with an equatorial crossing time of 1030 LT. As the ADEOS satellite passed over a scene, up to 14 successive measurements were acquired in eight narrow spectral bands located between 443 and 910 nm. The POLDER level 1 products routinely processed by CNES (the French Space Center) consist of calibrated radiances and Stokes parameters at full spatial resolution. The level-2 ERB and clouds product provides cloud properties (cloud amount, cloud optical thickness, cloud thermodynamic phase, cloud pressure, etc.) over ≈56 km × 56 km ''superpixel'' regions (≈9 × 9 full-resolution 6.2 km × 6.2 km POLDER pixels).

A detailed description of the ERB and clouds algorithm is given in Buriez et al. (1997) and Parol et al. (1999). The cloud detection scheme consists of a sequence of threshold tests based on reflectance R_λ (λ = 865 nm over ocean, 443 nm over land), 443 and 865 nm polarized radiance, and R_{763}/R_{765} and R_{443}/R_{865} ratio. Cloud optical thickness is estimated from 670 nm reflectance using a lookup table approach based on plane-parallel theory; a small modification was added to improve this estimation (see appendix). Cloud phase is derived from polarized reflectance at 865 nm. Cloud level pressure is derived using two different methods: the ''oxygen'' pressure is derived from absorption measurements in the oxygen-A band and the ''Rayleigh'' pressure is derived from spectral polarization measured at scattering angles ranging between 80° and 120°. Note that the algorithms are applied to each full-resolution POLDER pixel and direction but the whole results are averaged at the superpixel scale.

The analysis of the different ''directional'' values of cloud optical thickness is not very meaningful since a change in optical thickness by 1 can correspond to a change in cloud reflectance by 0.1 or 0.001, depending on whether the optical thickness is small or large. Instead, a logarithmic scale is often preferred (e.g., Pawlowska et al. 2000). Here we choose to make use of a representation, introduced in the ISCCP scheme, that is equivalent in radiative energy amount. Practically, the calculated parameter is the cloud visible spherical albedo. The spherical (or diffuse) albedo is obtained by integrating the reflectance over all viewing zenith, solar zenith, and relative azimuth angles, and is defined for a plane-parallel cloud layer over a black surface with no atmosphere. In other words, it represents the cloud reflectance independent of directional, surface, and atmospheric effects. Therefore it is a one-to-one function of the cloud optical thickness for a given microphysical model. In the POLDER processing scheme, this function (hereafter referred to as S_{10}) is calculated for a homogeneous cloud layer composed of liquid water droplets

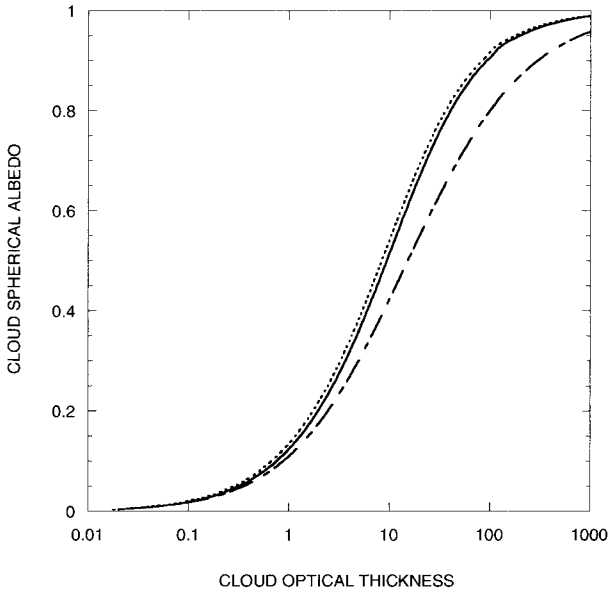

FIG. 1. Cloud visible spherical albedo as a function of optical thickness for various liquid water cloud models. The full line corresponds to a homogeneous cloud layer composed of droplets with an effective radius $r_e = 10$ μm. The dotted line corresponds to $r_e = 5$ μm. The long dashed line corresponds to the modelization introduced in section 5: a heterogeneous cloud scene is characterized by an exponential distribution function of cloud optical thickness (for this last case, the figure shows the relation between the mean spherical albedo and the mean optical thickness).

with an effective radius of 10 μm and an effective variance of 0.15 (Hansen and Travis 1974). It is also used in the ISCCP products where the cloud optical thickness values have linear increments in S_{10} (Rossow et al. 1996). As the basic measurements are radiances, the precision of the differences in spherical albedo is undoubtedly more easily interpretable than differences in optical thickness. Practically, cloud spherical albedo is directed inferred from the reflectance using a lookup table constructed from plane-parallel radiative transfer simulations for various cloud optical thickness; the one-to-one relation between spherical albedo and optical thickness is reported in Fig. 1.

In this study, 16 days (224 orbits) sampled throughout the 8 months of available POLDER data were selected: the 12th and 27th day of each month from November 1996 to June 1997. As we are concerned with the retrieval of cloud optical thickness (or spherical albedo) from liquid water clouds, we select the superpixels for which the thermodynamic phase is found to be liquid according to the observed polarization signature (Parol et al. 1999). We cannot totally exclude a cirrus contamination. However, polarization is known to correspond to the first orders of scattering and therefore to the highest layers of a cloud system. Therefore, it is unlikely that the contamination be strong enough to affect significantly the reflectance measurements when the polarization signature is found to correspond to liquid water clouds.

To avoid ambiguous cases, we exclude the directions within the expected region of solar specular reflection and the superpixels for which there is a risk of snow or sea-ice coverage according to the European Centre for Medium-Range Weather Forecasts analysis. Moreover, only superpixels that are declared totally cloudy in all viewing directions are considered since the cloud parameter retrieval is more uncertain for partly cloudy scenes. However, it should be noted that the actual cloud cover of the superpixels declared overcast can differ from 100% due to cloudiness variability at the subpixel scale.

Unlike the actual value of cloud optical thickness or spherical albedo, the retrieved directional values can depend on the solar and the viewing direction. To compare these different directional values, we plot their variation against scattering angle Θ. A given value of Θ can correspond to several combinations of (θ_s, θ_v, ϕ), where θ_s, θ_v, and ϕ are, respectively the solar zenith, the viewing zenith, and the relative azimuth angle, as reported in Fig. 2. For the POLDER observations, Θ roughly lies between 60° and 180°. We preserve only the superpixels that are viewed instantaneously by POLDER from at least 4 Θ directions: two with $\Theta < 120°$ and two with $\Theta > 120°$. Actually, almost all super-pixels (92%) are viewed from at least 10 directions.

Following the criteria of selection summarized in Table 1, a significant number of cloudy superpixels is preserved: 192 039 over ocean and 32 485 over land. Their latitudinal distribution is reported in Table 2. There are a lot of superpixels over ocean near 60°S. This is due to the frequent occurrence of low-level clouds in this region and to the overlap of successive POLDER tracks, which increases with latitude. The decrease in the number of superpixels at latitudes >60° is due to sea-ice and snow coverage. Moreover, POLDER observations are processed only for solar zenith angles <78.5°. The solar zenith angle is typically around 30° near the equator and 60° at higher latitudes.

The main properties of these selected superpixels are reported in Table 2. On average, the Rayleigh cloud pressure is 768 ± 154 hPa (mean ± standard deviation). The oxygen cloud pressure, which is known to be larger than the cloud-top pressure because of the photon penetration effect (Vanbauce et al. 1998), is 810 ± 111 hPa. The cloud spherical albedo is 0.53 ± 0.14, which corresponds to an optical thickness of ≈10 (see Fig. 1). The heterogeneity of a cloudy scene can be characterized by the spatial standard deviation in the retrieved cloud spherical albedo over the 9 × 9 pixels comprising a superpixel: it is 0.09 ± 0.04, which corresponds to a spatial variation in optical thickness of ≈4. Note that liquid water clouds appear higher and denser over land than over ocean, in good agreement with ISCCP observations (Rossow and Schiffer 1991).

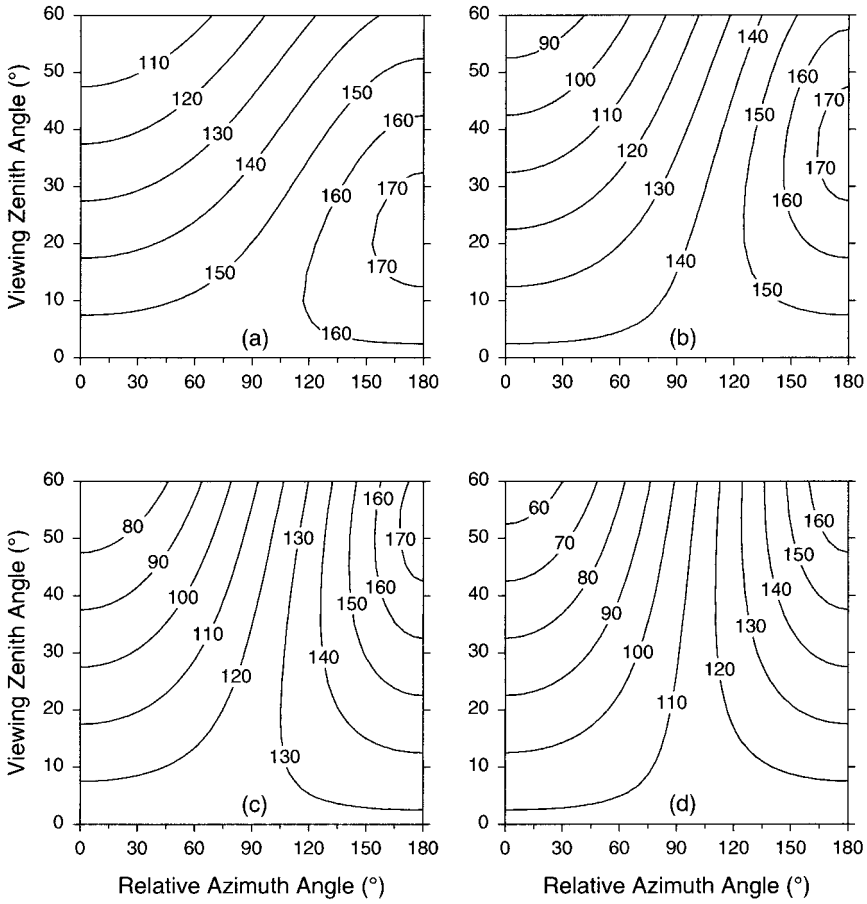

FIG. 2. Scattering angle vs viewing zenith and relative azimuth angle for (a) $\theta_s = 22.5°$, (b) $\theta_s = 37.5°$, (c) $\theta_s = 52.5°$, and (d) $\theta_s = 67.5°$.

3. Departure from the standard plane-parallel model

In the current version of the POLDER ERB and clouds algorithm, the cloudy pixels are assumed to be fully covered by a plane-parallel layer composed of liquid water droplets with an effective radius of 10 μm, as in the ISCCP analysis. As mentioned in the introduction, this approach can lead to substantial errors when used to infer cloud optical thickness from satellite measurements. This point is investigated by analyzing the angular variability in the retrieved cloud spherical albedo $S_{10}(\Theta)$. The dependency of this variability on various geophysical parameters is examined also.

TABLE 1. Criteria of selection applied to the POLDER superpixels.

Parameter	Condition
Cloud phase	Liquid
Cloud cover	Overcast
Snow or sea ice	No risk
Sunglint direction	Outside (by 30° over ocean and 1° over land)
Scattering angle	At least 2 angles $<120°$
	At least 2 angles $>120°$

Figure 3 shows the difference $S_{10}(\Theta) - S_{10}(120°)$, averaged over the whole dataset, between the directional value of cloud spherical albedo in the Θ-direction and its value at the reference scattering angle of 120°. Practically, for each superpixel, $S_{10}(120°)$ is interpolated from the two directional S_{10} values with Θ lying just below 120° and the two directional S_{10} values with Θ just above 120°. Then the difference $S_{10}(\Theta) - S_{10}(120°)$ is sorted into angular bins of width 2° between $\Theta = 60°$ and $\Theta = 180°$. The curve shown in Fig. 3 represents the mean difference (plus or minus one standard deviation) as a function of Θ in 2° steps. The full (dashed) lines correspond to mean differences such as $\sigma/\sqrt{N}$ is smaller (larger) than 0.0005, where σ and N are, respectively, the standard deviation and the number of measurements in the considered class of scattering angle. If all the samples are totally independent, $\sigma/\sqrt{N}$ represents the estimated error in the mean (Bevington and Robinson 1992). Although all the superpixels are not independent, full lines are expected to be more reliable than dashed ones. That ''precision'' is not to be confused with the accuracy, which is chiefly limited by the multiangular calibration within 1%, that means typ-

TABLE 2. Number and zonal characteristics (mean ± std dev) of the selected superpixels: solar zenith angle θ_s, Rayleigh cloud pressure P_{Ray}, oxygen cloud pressure P_{O_2}, cloud spherical albedo S_{10}, and spatial standard deviation of the cloud spherical albedo σ_S.

Latitudes	Number	θ_s	P_{Ray} (hPa)	P_{O_2} (hPa)	S_{10}	σ_S
(a) Over ocean						
60°–75°N	10 604	53° ± 8°	800 ± 119	894 ± 82	0.57 ± 0.15	0.07 ± 0.04
30°–60°N	30 440	51° ± 15°	769 ± 145	831 ± 106	0.51 ± 0.14	0.10 ± 0.04
0°–30°N	8903	39° ± 14°	699 ± 193	759 ± 149	0.48 ± 0.13	0.11 ± 0.04
0°–30°S	12 541	41° ± 12°	762 ± 191	798 ± 148	0.45 ± 0.12	0.10 ± 0.04
30°–60°S	93 895	53° ± 12°	793 ± 154	820 ± 108	0.51 ± 0.13	0.09 ± 0.04
60°–75°S	35 655	57° ± 8°	787 ± 119	806 ± 86	0.58 ± 0.13	0.08 ± 0.04
All	192 039	52° ± 13°	782 ± 151	820 ± 107	0.52 ± 0.14	0.09 ± 0.04
(b) Over land						
60°–75°N	3399	44° ± 3°	684 ± 117	765 ± 89	0.49 ± 0.13	0.10 ± 0.04
30°–60°N	14 961	46° ± 14°	705 ± 140	777 ± 100	0.58 ± 0.14	0.10 ± 0.04
0°–30°N	5117	36° ± 13°	660 ± 139	721 ± 125	0.55 ± 0.14	0.09 ± 0.04
0°–30°S	7627	35° ± 12°	674 ± 158	732 ± 133	0.51 ± 0.14	0.09 ± 0.03
30°–60°S	1381	51° ± 15°	715 ± 178	763 ± 136	0.51 ± 0.14	0.11 ± 0.04
60°–75°S	0	—	—	—	—	—
All	32 485	42° ± 14°	689 ± 145	756 ± 117	0.55 ± 0.14	0.10 ± 0.04

ically an uncertainty in spherical albedo of 0.005 (Hagolle et al. 1999). On the other hand, the calculation errors due to approximations or interpolations are estimated to be always smaller than this calibration uncertainty, except near the backscattering direction since the reflectance can vary very sharply as the scattering angle tends toward 180°.

On average, the standard plane-parallel model is found to be fairly representative of liquid water cloud anisotropy at moderate solar zenith angles, as previously reported by Parol et al. (1999). However, Fig. 3 confirms the weakness in the model in the rainbow direction ($\Theta \sim 140°$) and for the smallest observable values of scattering angle ($\Theta < 90°$). This behavior of $S_{10}(\Theta) - S_{10}(120°)$ remains the same when we select any latitudinal belt, the different curves (not shown) are mixed together within ±0.01. Otherwise, the weakness in the model appears to be more pronounced over land than over ocean. A detailed analysis shows that the differences between continental and maritime observations reported in Fig. 4 remain the same when we select any latitudinal belt, class of solar angle, cloud pressure, or cloud optical thickness. This may be related to the cloud microphysics. Indeed, cloud droplet radii in continental liquid water clouds are known to be smaller than in marine clouds (Han et al. 1994). In the following, results

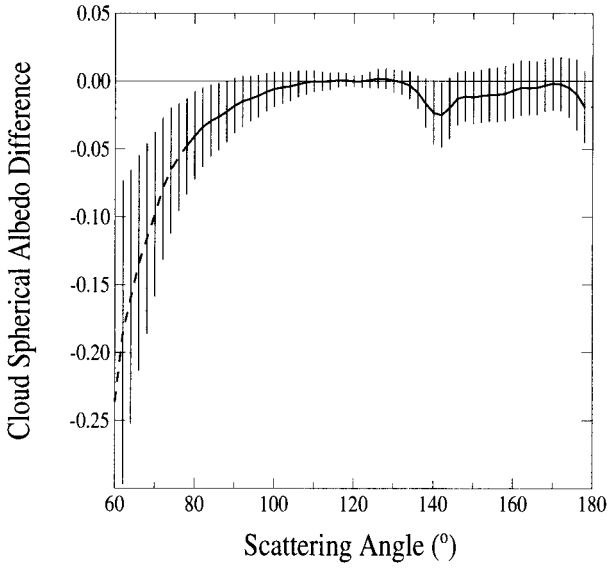

FIG. 3. Cloud spherical albedo difference $S_{10}(\Theta) - S_{10}(120°)$ as a function of scattering angle Θ, for the whole dataset. Directional values of cloud spherical albedo are retrieved by using the standard water droplet cloud model (with an effective radius of 10 μm). The bars correspond to plus or minus one standard deviation around the mean value by classes of 2°. The full lines correspond to ''precise'' mean differences.

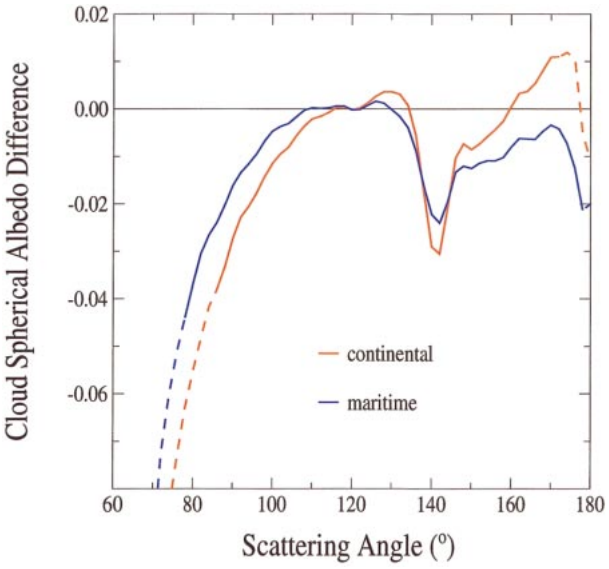

FIG. 4. Cloud spherical albedo difference $S_{10}(\Theta) - S_{10}(120°)$ as a function of scattering angle Θ, for the maritime and continental situations. The full lines correspond to precise mean differences.

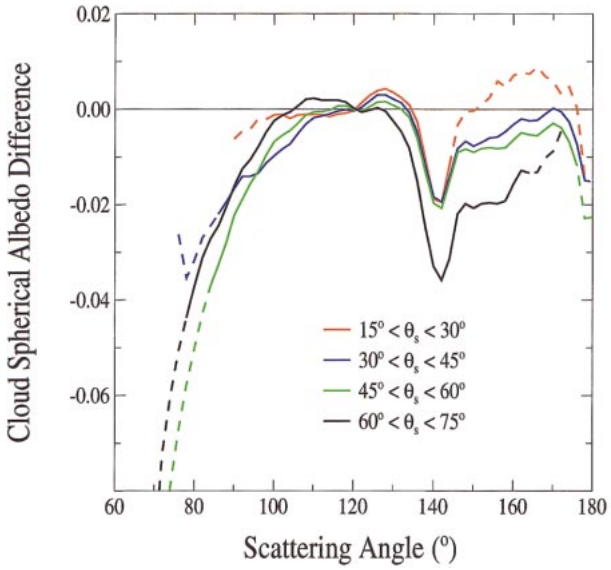

FIG. 5. As in Fig. 4 but for the whole dataset by classes of solar zenith angle.

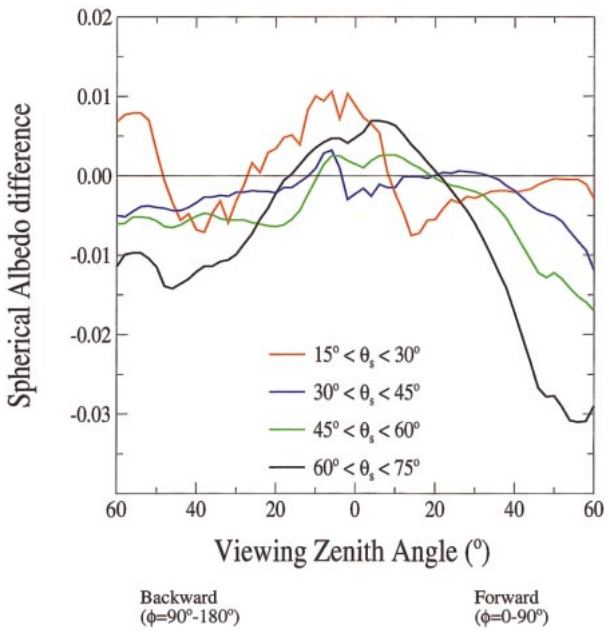

FIG. 6. Cloud spherical albedo difference $S_{10}(\Theta) - S_{10}(120°)$ as a function of viewing zenith angle θ_v, for the whole dataset by classes of solar zenith angle.

are discussed from the whole dataset without discrimination between continental and oceanic situations.

Figure 5 shows the mean difference $S_{10}(\Theta) - S_{10}(120°)$ as a function of Θ, for different classes of solar zenith angle. Overall, the largest differences in retrieved directional spherical albedos are observed for the largest values of θ_s. Figure 5 is rather hard to interpret since Θ depends on (θ_s, θ_v, ϕ) (see Fig. 2). A representation as a function of the viewing zenith angle θ_v is more usual, so the mean difference $S_{10}(\Theta) - S_{10}(120°)$ is also plotted versus θ_v in Fig. 6. This last figure is not very informative when $15° < \theta_s < 30°$: the mean difference is always weak (within ± 0.01), since the weakness due to the rainbow direction, which clearly appears in Fig. 5, is spread out in both the forward and the backward-scattering direction. For larger values of θ_s, one observes a decrease of $S_{10}(\Theta) - S_{10}(120°)$ as the viewing zenith angle increases, especially in the forward-scattering direction. At large solar zenith angles ($\theta_s > 60°$), this decrease is three times more important in the forward-scattering direction than in the backward one. This is consistent with results of Loeb and Coakley (1998), who found relative differences between plane-parallel model reflectances and AVHRR observations about two to three times larger in the forward-scattering direction than in the backscattering direction. Note that the comparison of Figs. 5 and 6 clearly shows that a representation as a function of the scattering angle highlights more the weakness of the plane-parallel model in the rainbow direction.

The influence of the cloud pressure is reported in Fig. 7 where the Rayleigh pressure P_{Ray} averaged over all the available viewing directions is considered. The plane-parallel cloud model appears more adequate as the clouds are lower. That is clearly related to the presence of stratus clouds at the lowest altitudes. Quite similar results are obtained when the oxygen pressure Po_2 is considered (not shown).

Figure 8 shows that the model is less suitable for small values of cloud optical thickness. This is clearly highlighted in the rainbow region. The difference $S_{10}(120°) - S_{10}(140°)$ is more than twice as large for optical thickness smaller than 3.6 ($\overline{S}_{10} < 0.3$, where $\overline{S}_{10}$ stands for the cloud spherical albedo averaged over all

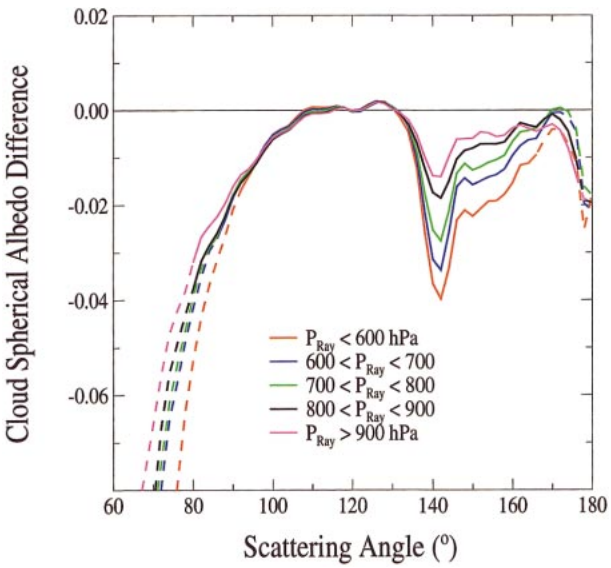

FIG. 7. As in Fig. 4 but for the whole dataset by classes of Rayleigh cloud pressure.

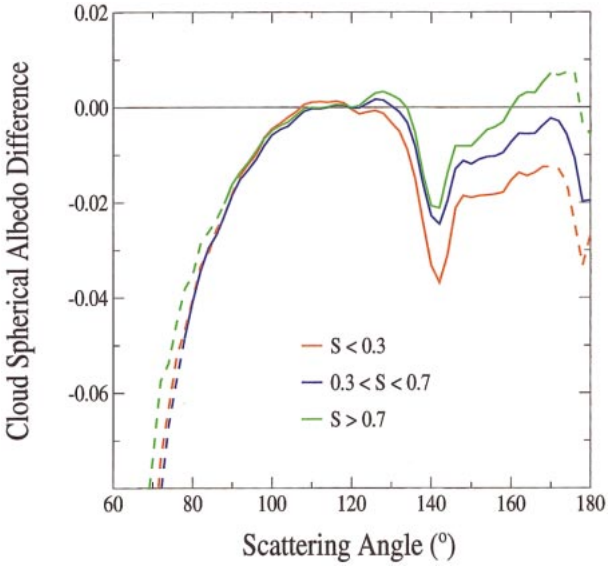

FIG. 8. As in Fig. 4 but for the whole dataset by classes of cloud spherical albedo.

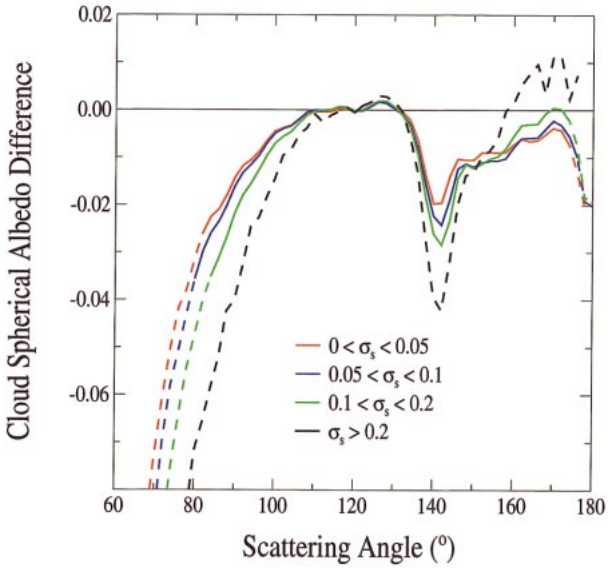

FIG. 9. As in Fig. 4 but for the whole dataset by classes of spatial standard deviation of the cloud spherical albedo over the 9 × 9 pixels composing a superpixel.

angles) compared to optical thickness larger than 23 ($\overline{S}_{10} > 0.7$). This behavior can be related to differences in cloud type. Small values of optical thickness likely correspond to fractional cloud cover at the subpixel scale due to cumulus clouds. Large values are likely associated with extended clouds, that is, to stratiform clouds.

Figure 9 shows the angular variability of $S_{10}(\Theta) - S_{10}(120°)$ with respect to different classes of spatial heterogeneity. As mentioned above, the heterogeneity of a cloudy scene is characterized by the spatial standard deviation of the retrieved cloud spherical albedo over the 9 × 9 pixels composing a superpixel. The higher the spatial standard deviation, the more heterogeneous the clouds. Figure 9 confirms that the plane-parallel approximation becomes worse with increasing cloud heterogeneity.

4. Influence of the cloud droplet size

As mentioned above, cloud spherical albedos retrieved with the standard plane-parallel model are too small in the rainbow direction. This suggests that the cloud particle size is too large in the model. Therefore, we now consider a cloud particle distribution with an effective radius of 5 μm (instead of 10 μm) and the same effective variance of 0.15. An effective radius of about 5 μm is often encountered in stratus clouds (Stephens 1978) but is likely too small for global applications. Indeed the average was found to be around 10–12 μm over ocean and 7–9 μm over land both from AVHRR visible and infrared measurements (Han et al. 1994) and from POLDER polarization measurements (Bréon and Colzy 2000).

A new scattering phase function was thus computed for a particle size distribution with an effective droplet radius of 5 μm using Mie theory. Decreasing the effective droplet radius flattens the phase function somewhat in the rainbow direction (see Fig. 10) and produces a smaller peak in the forward-scattering direction (not shown). The POLDER data of the 16 selected days were then completely reprocessed in a similar way as in the

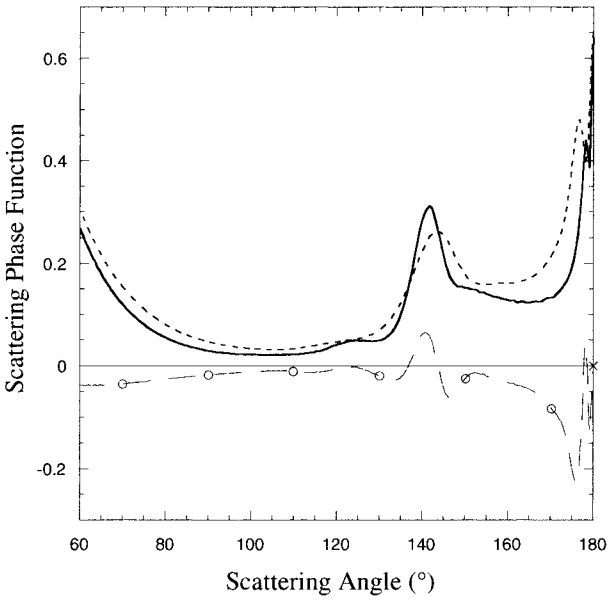

FIG. 10. Comparison of the scattering phase functions for water droplet distributions with an effective radius of 10 μm (full line) and 5 μm (dotted line), respectively. The phase function difference (10 − 5 μm) is represented by a long dashed line with open circles. For comparison with Fig. 10, the scattering angle range is limited to 60°–180°.

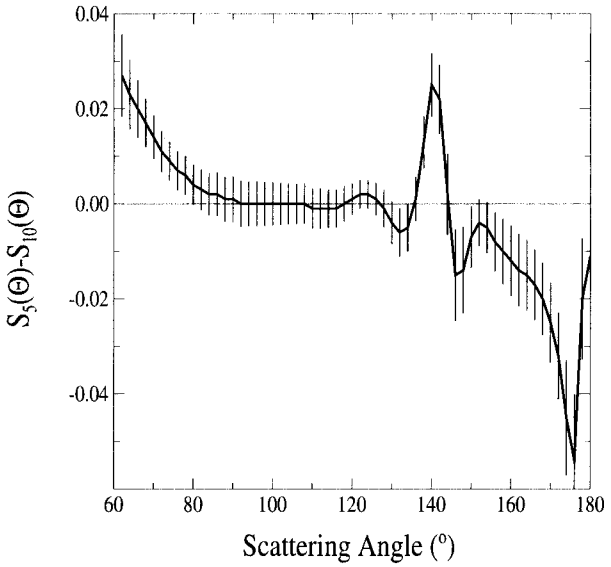

FIG. 11. Difference $S_5(\Theta) - S_{10}(\Theta)$ between the directional spherical albedo retrieved with the 5-μm model and the 10-μm model, respectively, as a function of scattering angle Θ, for the whole dataset. The bars correspond to plus or minus one std dev around the mean.

operational ERB and clouds algorithm but with the new phase function.

On average, the spherical albedos retrieved with the 10-μm model and the 5-μm model are nearly the same; the overall mean difference is only 0.001. However, the relation between spherical albedo and optical thickness depends on the particle size distribution (see Fig. 1). For a given value of spherical albedo, cloud optical thickness has to be multiplied by 0.89 when the droplet effective radius decreases from 10 to 5 μm (Han et al. 1994). Therefore, when changing the microphysical model a zero difference in cloud spherical albedo corresponds to an 11% difference in retrieved cloud optical thickness.

Figure 11 shows the angular variation of the difference $S_5(\Theta) - S_{10}(\Theta)$ between the directional spherical albedo retrieved with the 5-μm model and with the 10-μm model, respectively. The difference depends on the solar and viewing directions as well as on the magnitude of the cloud reflectance. However, for a fixed value of scattering angle this dependence is weak; the corresponding variability of the $S_5(\Theta) - S_{10}(\Theta)$ around the mean difference is small, typically ± 0.005. As expected, $S_5(\Theta) - S_{10}(\Theta)$ clearly varies as $P_{10}(\Theta) - P_5(\Theta)$ for large values of the scattering angle, say $\Theta > 100°$ (cf. Fig. 11 to Fig. 10). More surprisingly, when Θ decreases from 100° to 60°, $S_5(\Theta) - S_{10}(\Theta)$ increases while $P_{10}(\Theta) - P_5(\Theta)$ decreases. That is related to the fact that the forward peak of scattering is sharper for large water spheres and the more the scattering angle decreases, the more the viewing direction moves closer to the forward direction.

The differences between the directional values of

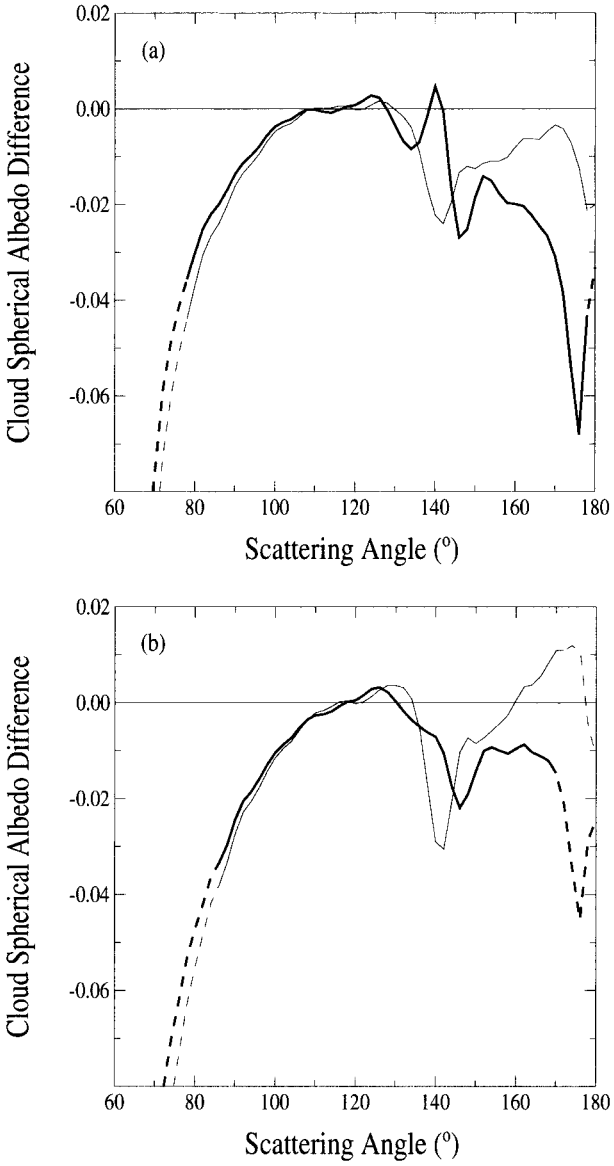

FIG. 12. Difference between the directional values of cloud spherical albedo and the reference value at 120° as a function of scattering angle Θ, for the (a) maritime and (b) continental situations. The thick lines correspond to the 5-μm model and the thin lines to the 10-μm model. The full lines correspond to precise mean differences.

cloud spherical albedo $S_5(\Theta)$ and the reference value $S_5(120°)$ are reported for maritime and continental situations in Figs. 12a and 12b, respectively. As expected, the 5-μm model is more suitable than the standard 10-μm model for scattering angle very close to 140°. But, it is hardly more convenient for small scattering angles and for maritime situations, quite less adequate for scattering angles beyond 150°. The better overall agreement would correspond to an effective radius intermediate between 5 and 10 μm over land and rather close to 10 μm over ocean. That is in agreement with previous studies (Han et al. 1994; Bréon and Colzy 2000). Moreover,

it clearly appears that any realistic value of droplet size cannot explain the observations for the smallest values of scattering angle under the assumption of the homogeneous plane-parallel model.

In the foregoing, the plane-parallel cloud layer is assumed vertically homogeneous. As the effective radius of cloud droplets generally increases with height (e.g., Gerber 1996), one can question whether this vertical variability can significantly affect the retrieval of cloud optical thickness as a function of scattering angle. Following Nakajima and King (1990), for typical distributions of droplet size the effect of this vertical stratification induces an overestimation of the cloud optical thickness by no more than 3% and moreover this error is not very dependent on the observational angles. To be sure, we computed the reflectance of an adiabatic cloud model with a typical optical thickness of 10, for a solar zenith angle of 60°: the liquid water content w increases linearly with height and the effective radius of droplets increases as $w^{1/3}$ up to 10 μm at the cloud top. We inverted the reflectance values by assuming an effective radius of 10 μm constant throughout the whole cloud. The retrieved cloud optical thickness is then 10.32 at nadir ($\Theta = 120°$) and decreases only down to 10.25 in the forward direction ($\Theta = 60°$). That corresponds to a $S_{10}(60°) - S_{10}(120°)$ difference weaker than 0.002, which is quite negligible. Consequently, any realistic microphysics of liquid water cloud appears to be definitely insufficient to explain the decrease of the retrieved optical thickness in the forward direction.

5. Influence of cloud heterogeneities

Heterogeneities in cloud properties can have a large impact on cloud bidirectional reflectances. They can occur because of horizontal variations in cloud liquid water path or because of the variations in cloud shape (finite clouds or simply nonflat cloud tops). Using the independent pixel approximation (IPA) (Cahalan et al. 1994), which is the simplest extension of plane-parallel radiative transfer, we only consider horizontal variations in liquid water path and neglect net horizontal photon transport.

From high spatial resolution Landsat imagery of marine boundary layer clouds, Barker et al. (1996) showed that the distributions of optical thickness can often be approximated by the gamma distribution function,

$$p(\tau) = \frac{1}{\Gamma(\nu)}\left(\frac{\nu}{\langle\tau\rangle}\right)^{\nu}\tau^{\nu-1}e^{-\nu\tau/\langle\tau\rangle}, \tag{1}$$

where $p(\tau)$ is the normalized distribution function of cloud optical thickness, $\Gamma(\nu)$ is the gamma function, and $\nu = (\langle\tau\rangle/\sigma)^2$ in which $\langle\tau\rangle$ and σ are mean and standard deviation of τ, respectively. In order to investigate the effect of horizontal variations of cloud optical thickness on cloud property retrievals, we make use of this approximation for all the POLDER pixels identified as liquid water clouds and choose $\nu = 1$. This value is representative of heterogeneous cloudy scenes such as broken clouds rather than overcast stratocumulus clouds and therefore that would correspond to a high degree of heterogeneity at the global scale.

The reflectance of a POLDER full-resolution pixel is then assumed to be

$$\langle R\rangle = \int_0^{\infty} p(\tau)R_{\rm pp}(\tau)\,d\tau, \tag{2}$$

where $R_{\rm pp}(\tau)$ is the reflectance of a plane-parallel layer of optical thickness τ. Practically $\langle R\rangle$ is approximated with $\nu = 1$ by

$$\begin{aligned}\langle R\rangle &= \sum_i R_{\rm pp}(\tau_i)\int_{(\tau_{i-1}+\tau_i)/2}^{(\tau_i+\tau_{i+1})/2} p(\tau)\,d\tau \\ &= \sum_i R_{\rm pp}(\tau_i)\left[\exp\left(-\frac{\tau_{i-1}+\tau_i}{2\langle\tau\rangle}\right) - \exp\left(-\frac{\tau_i+\tau_{i+1}}{2\langle\tau\rangle}\right)\right],\end{aligned} \tag{3}$$

where two successive values of optical thickness τ_i correspond to a 0.004 increment in spherical albedo.

The POLDER data of the 16 selected days were again processed by replacing the lookup table of R versus τ by a new lookup table of $\langle R\rangle$ versus $\langle\tau\rangle$, by considering cloud droplets with an effective radius of 10 μm as in the standard model. Now, the relation between the mean cloud spherical albedo $\langle S_{10}\rangle$ and the mean optical thickness $\langle\tau\rangle$ significantly differs from that of the homogeneous case, as shown in Fig. 1. For example, a cloud spherical albedo of 0.3 corresponds to a mean optical thickness $\langle\tau\rangle = 4.9$ in the inhomogeneous case instead of $\tau = 3.6$ in the homogeneous case. This difference increases with the albedo: a cloud spherical albedo of 0.7 corresponds to $\langle\tau\rangle = 48$ instead of $\tau = 23$. The angular variation of the difference $S_{10,\rm INH}(\Theta) - S_{10}(\Theta)$ between the directional spherical albedo retrieved with the inhomogeneous cloud model and with the homogeneous one, respectively, is shown in Fig. 13. For a fixed value of scattering angle, the variability of the $S_{10,\rm INH}(\Theta) - S_{10}(\Theta)$ around the mean difference is typically ± 0.01. The difference $S_{10,\rm INH}(\Theta) - S_{10}(\Theta)$ remains always small for large scattering angles but becomes quite significant when Θ decreases down to 60°.

The difference between the directional values of cloud spherical albedo $S_{10,\rm INH}(\Theta)$ and the reference value $S_{10,\rm INH}(120°)$ is reported in Figs. 14a and 14b. The inhomogeneous cloud model provides results that are more self-consistent than the homogeneous one. That is obvious from Fig. 14a for maritime situations. This improvement chiefly concerns the observations corresponding to low solar elevations and/or to high spatial variations over the 9×9 pixels composing a superpixel. For continental situations, the better agreement would be obtained for the inhomogeneous model with

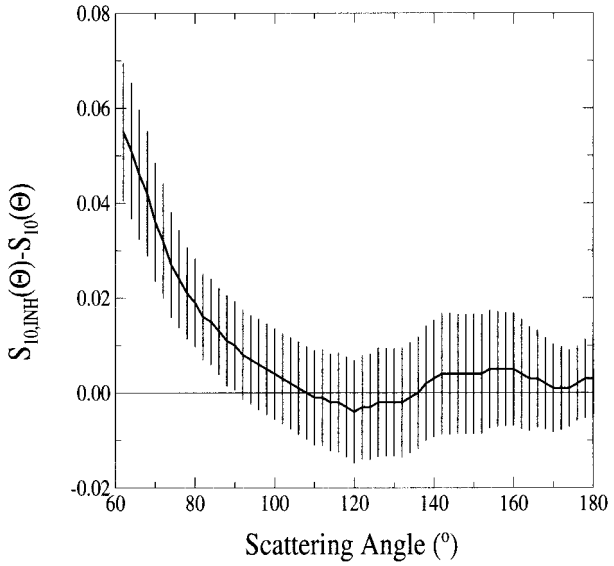

FIG. 13. Difference $S_{10,\mathrm{INH}}(\Theta) - S_{10}(\Theta)$ between the directional spherical albedo retrieved with the inhomogeneous and the homogeneous cloud model, respectively, as a function of scattering angle Θ, for the whole dataset. The bars correspond to plus or minus one standard deviation around the mean.

a smaller effective radius of cloud particles (combine Figs. 12b and 14b). Overall, the inhomogeneous cloud model could be considered as acceptable for scattering angle values down to ~80°. However, a too large departure remains for smaller values of scattering angle. In view of the high degree of heterogeneity of the considered cloud model ($\nu = 1$), it does not seem realistic to assume that only horizontal variations in cloud optical thickness can explain such a departure. A similar conclusion was obtained from theory in Loeb et al. (1998), who argued that cloud-top height variability is responsible for the marked angular dependence in plane-parallel model errors, particularly for large solar zenith angles in the forward-scattering direction.

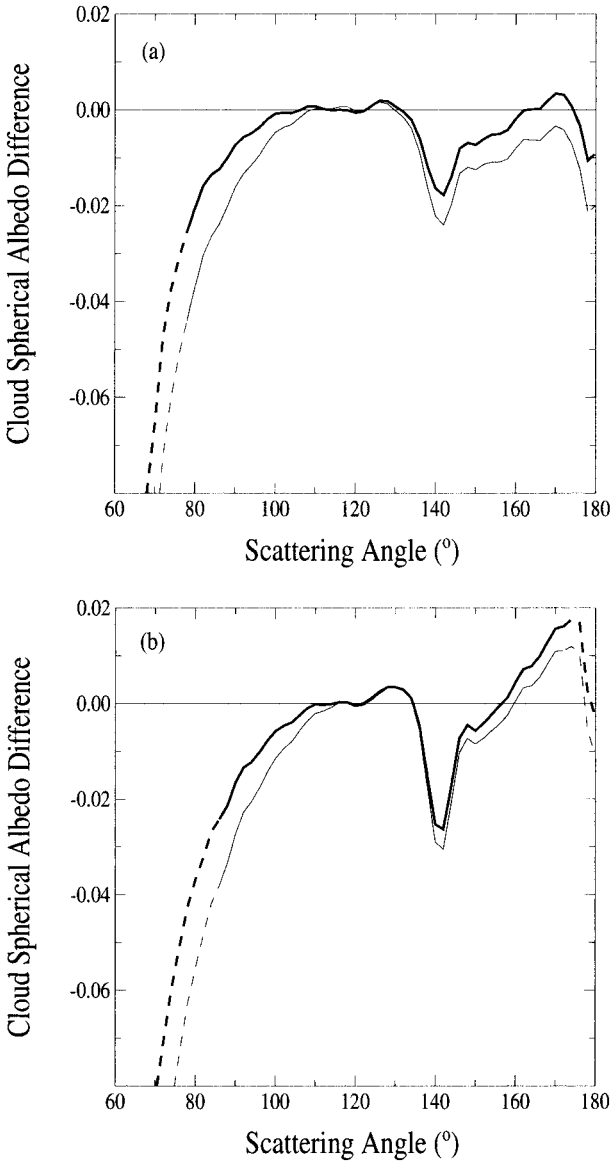

FIG. 14. Difference between the directional values of cloud spherical albedo and the reference value at 120° as a function of scattering angle Θ, for the (a) maritime and (b) continental situations. The thick lines correspond to the inhomogeneous cloud model and the thin lines to the homogeneous cloud model. The full lines correspond to precise mean differences.

6. Conclusions

The usual plane-parallel cloud model composed of liquid water droplets was compared to ADEOS–POLDER observations: 225 524 sequences of about a dozen bidirectional reflectances measured in the 670-nm channel were selected through the November 1996–June 1997 period. All of these observations correspond to totally cloudy superpixels composed of about 9×9 pixels for which the thermodynamic phase is liquid according to the observed polarization signature at 865 nm. These clouds are low (typically around 800 hPa) and bright (generally within 40%–70% in reflectivity).

The plane-parallel model is used to infer cloud visible spherical albedo from directional POLDER measurements. The cloud spherical albedo is a monotonic function of cloud optical thickness for a given microphysical model, and is representative of the cloud reflectance relieved of both the directional and the surface and atmospheric effects. In the operational POLDER processing scheme, the cloud spherical albedo is retrieved from bidirectional reflectance measurements by assuming a homogeneous cloud layer composed of liquid water droplets with an effective radius of 10 μm as in the ISCCP scheme. This model represents liquid water clouds rather well at moderate solar zenith angles. However, significant differences between model and observations appear in the rainbow direction and for the smallest observable values of scattering angle ($\Theta <$

90°). These results are consistent with those of Loeb and Coakley (1998), who found large differences between plane-parallel model calculations and satellite observations for $\Theta < 90°$ based on AVHRR measurements from low-level marine stratus cloud layers.

The whole dataset was reprocessed by assuming a droplet effective radius of 5 μm instead of 10 μm. Changing the water droplet distribution does not lead to a significant improvement for maritime situations. On the other hand, a better overall agreement would be obtained with an effective radius intermediate between 5 and 10 μm for the continental liquid water clouds.

The dataset was also reprocessed by assuming a cloud optical thickness distribution with a standard deviation as large as the mean at the pixel scale. When the gamma IPA approximation of Barker et al. (1996) is used, an improvement is obtained, but it remains weak at least for realistic variations in cloud optical thickness.

The major deficiency of the various models based on the plane-parallel radiative transfer is observed for small values of the scattering angle, that is, in the forward-scattering direction at moderate to low solar elevations. From Monte Carlo simulations comparing 3D model radiances to 1D model ones, Loeb et al. (1998) showed that for these directions, the reflectance is very sensitive to subpixel-scale variations in cloud-top height (i.e., cloud bumps). It results in 3D model reflectances largely smaller than 1D values in the forward-scattering direction while the 3D-1D differences are noticeably reduced at other geometries (e.g., nadir view, backscattering direction).

One can argue that 3D models tend to produce rather stronger backscattered radiances than plane-parallel models, leading to an overestimation of optical thickness in opposition to Fig. 3. However, this enhancement of backscattering radiances is not systematically obtained from 3D models (e.g., Loeb et al. 1998, their Fig. 8a). Moreover, the retrieved cloud optical thickness notably depends on the assumed cloud microphysics (see Fig. 11). Our feeling is that the differences between the plane parallel model and the observations could be drastically reduced at backscattering angles by adjusting the microphysics of the model at the pixel scale. On the contrary, the differences observed in the forward-scattering direction support the idea that cloud-top height variations have to be taken into account.

Acknowledgments. The authors would like to thank Françoise Hennequart for reprocessing POLDER data and Bernard Bonnel for phase function calculations. This work was funded by CNES and the Région Nord-Pas de Calais. Information on the POLDER data can be found on online at http://polder@www-projet.cnes.fr:8060/.

APPENDIX

Cloud Optical Thickness Derivation

In the ERB and clouds algorithm (Buriez et al. 1997), the cloud optical thickness (or equivalently, the cloud spherical albedo) is estimated from the measured 670-nm reflectance using a lookup table approach. Offline calculations of reflectance are performed by using the discrete ordinate method with 40 discrete streams after truncating the forward peak of the phase function. These calculations are performed for 20 values of cloud spherical albedo, 10 values of surface albedo, and various conditions of viewing/illumination geometry: $\mu_s = \cos\theta_s$ varies from 0.2 to 1.0 by 0.025, $\mu_v = \cos\theta_v$ varies from 0.325 to 1.0 by 0.025, and ϕ varies from 0° to 180° by 5°. Simulations performed for other viewing conditions and/or with 380 discrete streams show errors in retrieved cloud spherical albedo weaker than ± 0.002 for directions for which the phase function is smooth. However, these errors can be noticeably larger (up to 0.04) near the rainbow and backscattering directions ($\Theta \approx 140°$ and 180°, respectively).

As such large errors due to interpolation between angle nodes are related to large angular variations in the reflectance part due to the first order of scattering $R_1(\Theta)$, we improve the estimate of the cloud optical thickness in the following way: while in the operational algorithm the reflectance R is interpolated between angle nodes, in the present version only the difference $R - R_1$ is interpolated and the reflectance $R_1(\Theta)$ due to the first order of scattering is calculated ''exactly'' for the scattering angle Θ of the observation. It results in a drastic decrease of the largest errors in cloud spherical albedo. Overall, the errors are expected to be less than 0.01 for individual pixels and less than 0.002 for mean spherical albedo differences as presented in this paper.

REFERENCES

Barker, H. W., B. A. Wielicki, and L. Parker, 1996: A parameterization for computing grid-averaged solar fluxes for inhomogeneous marine boundary layer clouds. Part II: Validation using satellite data. *J. Atmos. Sci.,* **53,** 2304–2316.

Bevington, P. R., and D. K. Robinson, 1992: *Data Reduction and Error Analysis for the Physical Sciences.* McGraw-Hill, 328 pp.

Bréon, F. M., and S. Colzy, 2000: Global distribution of cloud droplet effective radius from POLDER polarization measurements. *Geophys. Res. Lett.,* **27,** 4065–4068.

Buriez, J. C., and Coauthors, 1997: Cloud detection and derivation of cloud properties from POLDER. *Int. J. Remote Sens.,* **18,** 2785–2813.

Cahalan, R. F., 1994: Bounded cascade clouds: Albedo and effective thickness. *Nonlinear Processes Geophys.,* **1,** 156–167.

——, W. Ridgway, W. J. Wiscombe, S. Gollmer, and Harshvardhan, 1994: Independent pixel and Monte Carlo estimates of stratocumulus albedo. *J. Atmos. Sci.,* **51,** 3776–3790.

Deschamps, P. Y., F. M. Bréon, M. Leroy, A. Podaire, A. Bricaud, J. C. Buriez, and G. Sèze, 1994: The POLDER mission: Instrument characteristics and scientific objectives. *IEEE Trans. Geosci. Remote Sens.,* **32,** 598–615.

Descloitres, J., F. Parol, and J. C. Buriez, 1995: On the validity of the plane-parallel approximation for cloud reflectances as measured from POLDER during ASTEX. *Ann. Geophys.,* **13,** 108–110.

——, J. C. Buriez, F. Parol, and Y. Fouquart, 1998: POLDER observations of cloud bidirectional reflectances compared to a plane-parallel model using the ISCCP cloud phase functions. *J. Geophys. Res.,* **103,** 11 411–11 418.

Doutriaux-Boucher, M., J. C. Buriez, G. Brogniez, L. C.-Labonnote, and A. J. Baran, 2000: Sensitivity of retrieved POLDER directional cloud optical thickness to various ice particle models. *Geophys. Res. Lett.,* **27,** 109–112.

Gerber, H., 1996: Microphysics of marine stratocumulus clouds with two drizzle modes. *J. Atmos. Sci.,* **53,** 1649–1662.

Hagolle, O., and Coauthors, 1999: Results of POLDER in-flight calibration. *IEEE Trans. Geosci. Remote Sens.,* **37,** 1550–1567.

Han, Q., W. B. Rossow, and A. A. Lacis, 1994: Near-global survey of effective droplet radii in liquid water clouds using ISCCP data. *J. Climate,* **7,** 465–497.

Hansen, J. E., and L. D. Travis, 1974: Light scattering in planetary atmospheres. *Space Sci. Rev.,* **16,** 527–610.

Loeb, N. G., and J. A. Coakley Jr., 1998: Inference of marine stratus cloud optical depths from satellite measurements: Does 1D theory apply? *J. Climate,* **11,** 215–233.

——, T. Várnai, and D. M. Winker, 1998: Influence of subpixel-scale cloud-top structure on reflectances from overcast stratiform cloud layers. *J. Atmos. Sci.,* **55,** 2960–2973.

Mishchenko, M. I., W. B. Rossow, A. Macke, and A. A. Lacis, 1996: Sensitivity of cirrus cloud albedo, bidirectional reflectance and optical thickness retrieval accuracy to ice particle shape. *J. Geophys. Res.,* **101,** 16 973–16 985.

Nakajima, T., and M. D. King, 1990: Determination of the optical thickness and effective particle radius of clouds from reflected solar radiation measurements. Part 1: Theory. *J. Atmos. Sci.,* **47,** 1878–1893.

Parol, F., J. C. Buriez, C. Vanbauce, P. Couvert, G. Sèze, P. Goloub, and S. Cheinet, 1999: First results of the POLDER ''Earth Radiation Budget and Clouds'' operational algorithm. *IEEE Trans. Geosci. Remote Sens.,* **37,** 1597–1612.

Pawlowska, H., and Coauthors, 2000: Microphysics/radiation interaction in a stratocumulus cloud: The EUCREX mission 206 case study. *Atmos. Res.,* **55,** 85–102.

Rossow, W. B., and R. A. Schiffer, 1991: ISCCP cloud data product. *Bull. Amer. Meteor. Soc.,* **72,** 2–20.

——, A. W. Walker, D. E. Beuschel, and M. D. Roiter, 1996: International Satellite Cloud Climatology Project (ISCCP): Documentation of new cloud datasets. WMO Note WMO/TD-737, 115 pp.

Stephens, G. L., 1978: Radiation profiles in extended water clouds. I: Theory. *J. Atmos. Sci.,* **35,** 2111–2122.

Vanbauce, C., J. C. Buriez, F. Parol, B. Bonnel, G. Sèze, and P. Couvert, 1998: Apparent pressure derived from ADEOS-POLDER observations in the oxygen A-band over ocean. *Geophys. Res. Lett.,* **25,** 3159–3162.